ADVANCED MATERIALS TECHNOLOGIES
www.advmattechnol.de

Integration of Organic Electrochemical Transistors with Implantable Probes

*Sanggil Han, Anastasios G. Polyravas, Shofarul Wustoni, Sahika Inal, and George G. Malliaras**

Organic electrochemical transistors (OECTs) are widely used as amplifying transducers of biological signals due to their high transconductance and biocompatibility. For implantable applications that penetrate into tissue, OECTs need to be integrated onto narrow probes. The scarcity of real estate necessitates the use of small local gate electrodes and narrow interconnects. This work shows that both of these factors lead to a decrease in the maximum transconductance and an increase in gate voltage required to attain this maximum. This work further shows that coating the gate electrode with a thick conducting polymer improves performance. These findings help guide the development of efficient OECTs on implantable probes.

1. Introduction

Organic electrochemical transistors (OECTs) have been employed as amplifying transducers in a host of applications,[1–4] including biosensors[5–9] and electrophysiology.[10–13] These devices incorporate an electrolyte between the gate electrode and the channel, which enables facile integration with biological systems.[14–16] A modulation in the gate voltage, V_G, by a biological event leads to a change in the drain current, I_D. As the signal is transduced, its power is amplified by a factor that depends on the transconductance, $g_m = \partial I_D/\partial V_G$.[15] An identifying characteristic of OECTs is that changes in doping take place throughout the entire volume of the channel, contrary to field-effect transistors (FETs), in which doping changes only occur in a thin interfacial region adjacent to the gate dielectric.[1] This leads to a large I_D modulation and thus a high g_m, which makes OECTs excellent amplifying transducers.[1,14–17] Moreover, the fact that gating is mediated by an electrolyte enables the fabrication of simple-to-fabricate planar device architectures where the gate electrode is patterned next to the channel.[5–7]

To understand gating of OECTs, two capacitors related to the gate (C_G) and channel (C_{CH}) interfaces with the electrolyte need to be considered. As these capacitors are in series, the largest fraction of the applied V_G drops across the smallest capacitor. Therefore, for efficient gating, C_G must be much larger than C_{CH}, otherwise most of V_G drops at the gate/electrolyte interface.[1,18] This implies that the majority of the footprint of the transistor should be devoted to the gate electrode. Alternatively, a non-polarizable gate electrode (e.g., Ag/AgCl pellet) that shows no voltage drop across its interface with the electrolyte can be used.[14–17] Ag/AgCl gate electrodes, however, add complexity to the fabrication process, make biofunctionalization difficult, and preclude use in implantable applications. Another particularity of OECTs is that they draw a large drain current, as the entire thickness of the channel (as opposed to a thin interfacial region in FETs) is involved in electronic carrier transport between source and drain.[19] This can lead to a significant fraction of the applied drain and gate voltage dropping on the interconnects[20,21] and places substantial demands on the design of the latter.

In neuroscience, while a global gate is often used to record electrophysiology with OECT arrays,[10] there are some applications that require a local gate configuration. This includes monitoring local changes in metabolites (e.g., glucose and lactate levels) using OECT arrays where biorecognition elements (such as enzymes) are attached on the gate electrodes.[6] In implantable applications, however, OECTs need to be fabricated on narrow probes, which means that they inevitably have small local gate electrodes and narrow interconnects. A typical implantable probe for neuroscience research will have a length of the order of tens of mm to reach deep brain structures, and a width of the order of 100–200 μm to minimize foreign body response while allowing a reasonable number of devices to be inserted into the brain.[13,22] As a result, interconnects have widths of the order of 10 μm or below, which leads to significant values of resistance. It is therefore important to evaluate the effects of small gates and narrow interconnects on

S. Han, A. G. Polyravas, G. G. Malliaras
Electrical Engineering Division
Department of Engineering
University of Cambridge
9 JJ Thomson Ave, Cambridge CB3 0FA, UK
E-mail: gm603@cam.ac.uk

S. Wustoni, S. Inal
Organic Bioelectronics Laboratory, Biological and Environmental Science and Engineering Division (BESE)
King Abdullah University of Science and Technology (KAUST)
Thuwal 23955-6900, Saudi Arabia

The ORCID identification number(s) for the author(s) of this article can be found under https://doi.org/10.1002/admt.202100763.

DOI: 10.1002/admt.202100763

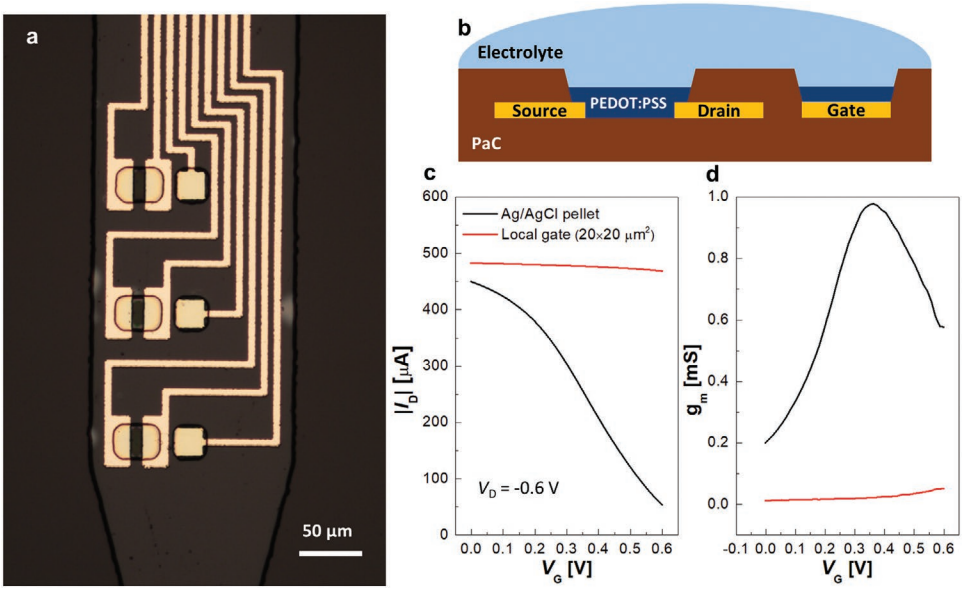

Figure 1. a) Microscope image and b) schematic of the probe with three OECTs. c) Transfer characteristics and d) transconductance of the OECTs operated by the local PEDOT:PSS gate and an external Ag/AgCl gate at V_D of –0.6 V.

transistor performance and develop strategies to overcome limitations. Here, we fabricate OECTs on narrow probes and show that they exhibit a small transconductance and a large threshold voltage under local gating. As such, their amplification properties are diminished. We find that both factors (small gate, resistive interconnects) contribute to this trend and that coating the gate electrode with a thick conducting polymer improves performance.

2. Results and Discussion

2.1. Characteristics of Organic Electrochemical Transistors on Implantable Probes

Figure 1a shows the geometry of the tip of a probe containing three OECTs. The device fabrication involves the deposition and patterning of a 100 nm thick Au film (anchored to the parylene C substrate with a 5 nm thick Ti adhesion layer) that defines the interconnects. The interconnects have a width of 5 µm and an average length of 2 mm near the tip of the probe and widen to 10 µm for 15 mm away from the tip. The OECT channel length, determined by the separation between the Au source and drain electrodes, is 10 µm. An ≈100 nm thick film of the conducting polymer, poly(3,4-ethylenedioxythiophene) doped with poly(styrene sulfonate) (PEDOT:PSS), is patterned in islands to yield the channels (30×20 µm^2, including source/drain contact overlaps, each 10 µm) and the gate electrodes (20×20 µm^2) of the OECTs as seen in Figure 1a. A parylene-C film insulates the Au interconnects, allowing the electrolyte to come in contact only with the PEDOT:PSS channels and gate electrodes, as displayed in the schematic of Figure 1b.

Figure 1c shows the transfer curves of an OECT operated by two different gate electrodes: the local PEDOT:PSS gate electrode (red curve) and an external Ag/AgCl pellet (black curve). In the OECT gated with the Ag/AgCl electrode, all of the applied V_G drops at the channel/electrolyte interface, which leads to a large I_D modulation. A typical bell-shaped g_m curve[23] is observed for this device configuration in Figure 1d, with a peak value of $g_{m,max}$ = 980 µS at $V_{G(gm,max)}$ = 0.35 V, where $V_{G(gm,max)}$ denotes the gate voltage that corresponds to the maximum transconductance. It was also confirmed that there is negligible variation in individual device performance of OECTs on the implantable probe (Figure S1, Supporting Information). In the case of the local gate electrode, however, the modulation in I_D is very small and the resulting transconductance remains below 100 µS. Moreover, it seems that $V_{G(gm,max)}$ shifts to values larger than 0.6 V.

Given that the local gate electrode is of similar size to the channel, poor gating leading to a small transconductance is expected. At the same time, the interconnects have a resistance R_{inter} = 900 Ω, which is significant compared to that of the channel, R_{ch} = 400 Ω. For I_D of ≈–500 µA (red curve in Figure 1c), the total resistive loss across the interconnects is –0.45 V, which is significant compared to the applied drain voltage, V_D, of –0.6 V. In this case, it was also observed that a thicker PEDOT:PSS channel does not help improve device performance unless the interconnect resistance is mitigated (Figure S2, Supporting Information). As a result, it is important to separate the two effects and evaluate independently their impact on the observed results.

2.2. Effects of Small Gates and Resistive Interconnects

To independently evaluate the effects of a small gate, we made devices with wide (200 µm) and short (10 mm) interconnects with a small resistance of ≈20 Ω, and used different gate electrodes to test their performance. **Figure 2**a shows the g_m versus V_G curves of one of these OECTs measured using

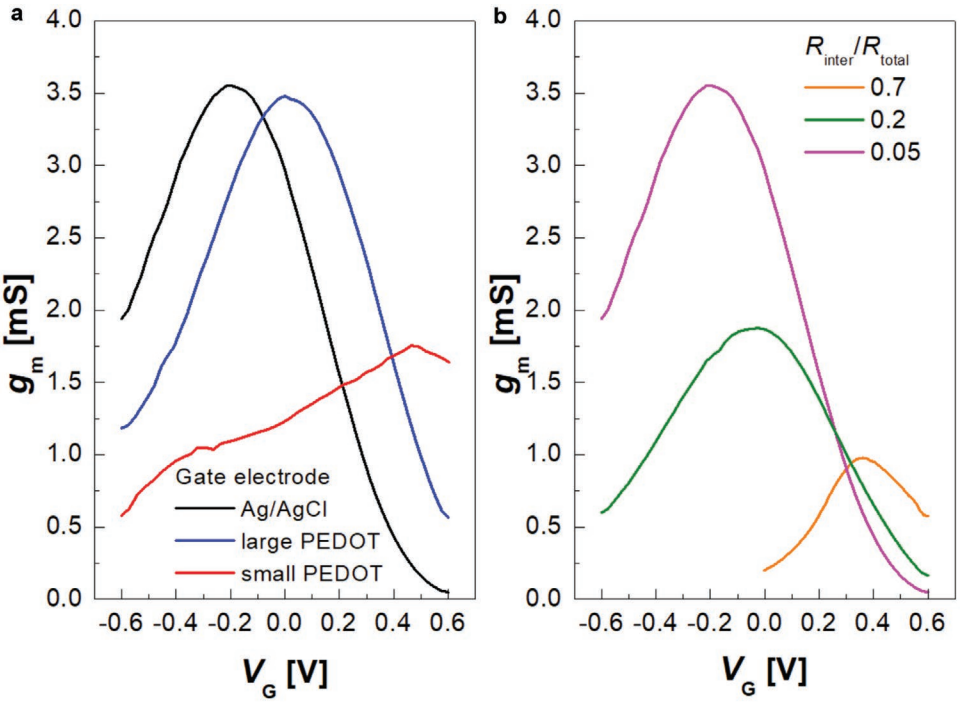

Figure 2. a) Transconductance of an OECT with interconnects of small resistance, operated by different gate electrodes: an Ag/AgCl pellet, large PEDOT:PSS gate (3×3 mm^2), and small PEDOT:PSS gate (same as the channel). b) Transconductance of OECTs, measured by an Ag/AgCl pellet, with different ratios of interconnect resistance to the total resistance, R_{inter}/R_{total}: 0.7, 0.2, and 0.05. All curves are measured at a fixed V_D of –0.6 V.

a small (0.1×0.1 mm^2) planar PEDOT:PSS gate (red), a large (3×3 mm^2) external PEDOT:PSS gate (blue), and an Ag/AgCl pellet (black). The results reveal that the small PEDOT:PSS gate not only decreases $g_{m,max}$ but also shifts $V_{G(gm,max)}$ to a higher voltage compared to the large PEDOT:PSS gate. The reduction in g_m is due to a significant decrease in the fraction of the applied V_G that drops on the channel, as predicted by the two-series capacitor model.[24] The poor gating also causes the maximum slope point of the transfer curve to be reached at a higher V_G, and thus results in the $V_{G(gm,max)}$ shift. It should be noted that the transistors with the Ag/AgCl and the large PEDOT:PSS gates have a similar $g_{m,max}$, but different $V_{G(gm,max)}$. This can be explained by a change in the threshold voltage due to the difference in work function between the two materials, as per previous reports.[25,26]

To independently evaluate the effects of resistive interconnects, we made devices with different ratios of interconnect resistance to the total resistance, R_{inter}/R_{total}, where R_{total} denotes the total resistance (interconnects and channel). All these OECTs were gated with an Ag/AgCl pellet. Figure 2b displays g_m versus V_G curves for OECTs with R_{inter}/R_{total} of 0.7 (orange curve), 0.2 (olive curve), and 0.05 (magenta curve). The data shows that resistive interconnects cause $g_{m,max}$ to decrease and $V_{G(gm,max)}$ to shift to high voltages, which agrees with previous simulation results.[21] These trends can be understood by the fact that resistive interconnects decrease both the true values of the drain and gate voltage compared to the applied V_D and V_G values. We find therefore that both small gates and resistive interconnects drive the same trend, namely a decrease in the values of transconductance that can be accessed in implantable OECTs.

2.3. Poly(3,4-Ethylenedioxythiophene) Electropolymerization on Gate Electrodes

The poor gating issue can be overcome by increasing C_G compared to C_{CH}, and this can be achieved by means other than an increase in the gate electrode area. For example, it is known that in conducting polymers that show mixed ionic/electronic conductivity (such as PEDOT:PSS), capacitance scales with film thickness.[16] Here, in order to increase C_G while keeping the area of the gate electrode small, an electrochemical polymerization method was used to add a coating of PEDOT doped with perchlorate (ClO_4) only on the gate electrodes of the OECTs in the probe of Figure 1a. Electrochemical deposition allows the selective coating on only the gate electrode by simply applying an electrical potential to that electrode with respect to a reference electrode immersed in the solution. The number of electropolymerization cycles was varied between one, five, and nine consecutive scans (see Figure S3, Supporting Information, for the cyclic voltammetry curves recorded during electropolymerization), and the thickness of the electropolymerized PEDOT films was measured by a Stylus profilometry (Dektak XT, Bruker): 0.44 µm (one cycle), 2.6 µm (five cycles), 4.38 µm (nine cycles). The electrochemical impedance of the PEDOT:ClO_4-coated gate electrodes was measured in a saline solution as shown in **Figure 3**a, and C_G values were obtained from fits to a simplified Randles circuit:[16] 22 nF (one cycle), 122 nF (five cycles), 203 nF (nine cycles). The significant increase in C_G makes most of the applied V_G drop at the OECT channel (9 nF). This improves the transfer characteristics of the OECT (Figure 3b),

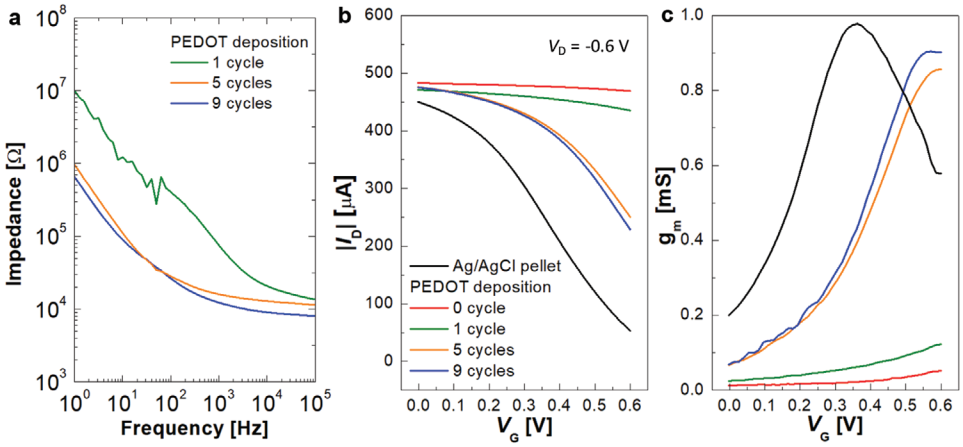

Figure 3. a) Bode plots of electrochemical impedance spectra of PEDOT:ClO_4-coated gate electrodes. b) Transfer characteristics and c) transconductance of the OECT operated by a PEDOT:ClO_4-coated gate electrode, with the different number of deposition cycles, and an Ag/AgCl pellet at V_D of −0.6 V.

and thus increases $g_{m,max}$ and decreases $V_{G(gm,max)}$ (Figure 3c). In addition, repetitive measurements were performed using new devices in a wider V_G range (0 V < V_G < 0.9 V) as seen in Figure S4, Supporting Information, which confirms that the findings presented here are reproducible.

2.4. Discussion

For implantable applications of OECTs, there are two issues: inefficient gating due to the small gate footprint and resistive interconnects. The former issue can be alleviated by an increase in C_G by means other than the footprint of the gate electrode. In addition to the conducting polymer coating approach demonstrated here, there are a few other ways to increase electrode capacitance, originally developed for neural electrode applications[27–29] For example, nanostructuring of the gate electrode surface (e.g., metal nanoparticles,[30] carbon nanotubes[27]) can increase effective surface area and lead to high C_G. Conducting polymer nanotubes[31] and nanocomposite films doped with carbon nanotubes[32,33] or graphene oxide[34] can also be used as coating materials for gate electrodes. The latter issue is more difficult to address. The use of multilayer probes can provide more space for interconnect lines but such probes come with increased fabrication complexity. Interconnect resistance can be minimized by the appropriate design of the complete probe. For instance, the part of the probe that does not penetrate into the brain can be designed to be wider. Thicker interconnects (to the limit imposed by fabrication and implantation constraints) can help further minimize interconnect resistance, but in general this is an issue that is hard to avoid altogether.

3. Conclusion

The scarcity of real estate on implantable probes creates two issues in OECT design: Local gate electrodes have a small footprint and interconnects are narrow. Using typical OECT structures, we showed that both issues lead to a reduction in the maximum transconductance and an increase in the gate voltage required to reach this maximum. Coating the gate electrode with a conducting polymer increases gate capacitance significantly and helps regain some of the lost performance. This work helps guide the design of efficient OECTs on implantable probes.

4. Experimental Section

Materials: PEDOT:PSS (Clevios PH1000) and Micro-90 solution were purchased from Heraeus and Cole–Parmer, respectively. Ethylene glycol, 4-dodecylbenzenesulfonic acid, (3-glycidyloxypropyl)trimethoxysilane, 3,4-ethylenedioxythiophene (EDOT), lithium perchlorate ($LiClO_4$) were acquired from Sigma-Aldrich and were used without further purification.

Device Fabrication and Characterization: The parylene probe with OECTs was fabricated based on previously reported procedures.[10,13,35] Briefly, a 2-μm-thick parylene film was first deposited on a 4-inch silicon wafer. Electrodes and interconnects were formed by depositing a Ti (5 nm)/Au (100 nm) layer using an e-beam evaporator (Kurt J Lesker PVD-75) with the aid of a lift-off process. The interconnects were completely covered by a 2-μm-thick second parylene layer. A sacrificial third parylene layer was deposited after spin-coating an anti-adhesive layer (2% v/v Micro-90 in deionized water). The OECT channels, gate electrodes, and contact pads were opened by photolithography and reactive ion etching (Oxford 80 Plasmalab plus). For preparing the PEDOT:PSS dispersion, a stock PEDOT:PSS solution (Clevios PH1000, Heraeus) was mixed with 5 vol% ethylene glycol, 0.25 vol% dodecyl benzene sulfonic acid, and 1 vol% (3-glycidoxypropyl)trimethoxysilane. The resulting dispersion was filtered through a 0.45 μm polytetrafluoroethylene filter, and then spin-coated at 3000 rpm. The OECT channels and gate electrodes were subsequently patterned by peeling off the sacrificial parylene layer, and then the wafer was baked at 130 °C for 60 min for PEDOT:PSS cross-linking. This was followed by immersing the wafer in deionized water overnight to remove any excess low-molecular weight compounds, and finally, the parylene probes with OECTs were peeled off from the wafer. The transfer characteristics of the OECTs were measured in a 0.01 M phosphate buffered saline solution by grounding the source electrode and applying a fixed V_D, V_D, of −0.6 V and V_G varying from 0 to +0.6 V using a semiconductor device analyzer (Keysight B1500A) inside a Faraday cage in ambient conditions. An Ag/AgCl pellet (World Precision Instruments) was used as a gate electrode in some experiments.

Poly(3,4-Ethylenedioxythiophene) Electropolymerization: For the preparation of the monomer aqueous dispersion, 10 mM EDOT and

100 mM $LiClO_4$ (as both counterions and supporting electrolyte) were mixed in deionized water with the aid of sonication at room temperature. The monomer aqueous solution was polymerized by cyclic voltammetry in the potential range between −0.01 and 1 V at a scan rate of 0.05 V s^{-1} using a three-electrode configuration coupled to an Autolab potentiostat (PGSTAT128N Metrohm): a planar gate of the OECTs as a working electrode, a Pt wire as a counter electrode, and Ag/AgCl (3 M NaCl) as a reference electrode. The electropolymerized film was then washed with deionized water and dried with nitrogen spray to remove any material that had weakly bound to the surface as well as unreacted monomers.

Supporting Information

Supporting Information is available from the Wiley Online Library or from the author.

Acknowledgements

This work was supported by the Natural Environment Research Council (NERC) under award No. NE/T012293/1, the European Union's Horizon 2020 Research and Innovation Programme under grant agreement No. 732032 (BrainCom), and the King Abdullah University of Science and Technology (KAUST) Office of Sponsored Research (OSR) under award No. OSR-2016-CRG5-3003.

Conflict of Interest

The authors declare no conflict of interest.

Data Availability Statement

The data that support the findings of this study are available from the corresponding author upon reasonable request.

Keywords

implantable electrodes, organic electrochemical transistors, transconductance

Received: June 23, 2021
Revised: July 23, 2021
Published online:

[1] J. Rivnay, S. Inal, A. Salleo, R. M. Owens, M. Berggren, G. G. Malliaras, *Nat. Rev. Mater.* **2018**, *3*, 17086.
[2] X. Strakosas, M. Bongo, R. M. Owens, *J. Appl. Polym. Sci.* **2015**, *132*, 41735.
[3] J. Liao, H. Si, X. Zhang, S. Lin, *Sensors* **2019**, *19*, 218.
[4] L. Bai, C. G. Elósegui, W. Li, P. Yu, J. Fei, L. Mao, *Front. Chem.* **2019**, *7*, 313.
[5] P. Lin, X. Luo, I-M. Hsing, F. Yan, *Adv. Mater.* **2011**, *23*, 4035.
[6] A.-M. Pappa, V. F. Curto, M. Braendlein, X. Strakosas, M. J. Donahue, M. Fiocchi, G. G. Malliaras, R. M. Owens, *Adv. Healthcare Mater.* **2016**, *5*, 2295.
[7] N. Saraf, E. R. Woods, M. Peppler, S. Seal, *Biosens. Bioelectron.* **2018**, *117*, 40.
[8] W. Hai, T. Goda, H. Takeuchi, S. Yamaoka, Y. Horiguchi, A. Matsumoto, Y. Miyahara, *Sens. Actuators, B* **2018**, *260*, 635.
[9] S. Han, S. Yamamoto, A. G. Polyravas, G. G. Malliaras, *Adv. Mater.* **2020**, *32*, 2004790.
[10] D. Khodagholy, T. Doublet, P. Quilichini, M. Gurfinkel, P. Leleux, A. Ghestem, E. Ismailova, T. Herve, S. Sanaur, C. Bernard, G. G. Malliaras, *Nat. Commun.* **2013**, *4*, 1575.
[11] A. Campana, T. Cramer, D. T. Simon, M. Berggren, F. Biscarini, *Adv. Mater.* **2014**, *26*, 3874.
[12] P. Leleux, J. Rivnay, T. Lonjaret, J.-M. Badier, C. Bénar, T. Hervé, P. Chauvel, G. G. Malliaras, *Adv. Healthcare Mater.* **2015**, *4*, 142.
[13] A. Williamson, M. Ferro, P. Leleux, E. Ismailova, A. Kaszas, T. Doublet, P. Quilichini, J. Rivnay, B. Rozsa, G. Katona, C. Bernard, G. G. Malliaras, *Adv. Mater.* **2015**, *27*, 4405.
[14] J. Rivnay, P. Leleux, M. Sessolo, D. Khodagholy, T. Hervé, M. Fiocchi, G. G. Malliaras, *Adv. Mater.* **2013**, *25*, 7010.
[15] D. Khodagholy, J. Rivnay, M. Sessolo, M. Gurfinkel, P. Leleux, L. H. Jimison, E. Stavrinidou, T. Herve, S. Sanaur, R. M. Owens, G. G. Malliaras, *Nat. Commun.* **2013**, *4*, 2133.
[16] J. Rivnay, P. Leleux, M. Ferro, M. Sessolo, A. Williamson, D. A. Koutsouras, D. Khodagholy, M. Ramuz, X. Strakosas, R. M. Owens, C. Benar, J.-M. Badier, C. Bernard, G. G. Malliaras, *Sci. Adv.* **2015**, *1*, e1400251.
[17] M. J. Donahue, A. Williamson, X. Strakosas, J. T. Friedlein, R. R. Mcleod, H. Gleskova, G. G. Malliaras, *Adv. Mater.* **2018**, *30*, 1705031.
[18] O. Yaghmazadeh, F. Cicoira, D. A. Bernards, S. Y. Yang, Y. Bonnassieux, G. G. Malliaras, *J. Polym. Sci., Part B: Polym. Phys.* **2011**, *49*, 34.
[19] D.A. Bernards, G.G. Malliaras, *Adv. Funct. Mater.* **2007**, *17*, 3538.
[20] A. G. Polyravas, N. Schaefer, V. F. Curto, A. B. Calia, A. Guimera-Brunet, J. A. Garrido, G. G. Malliaras, *Appl. Phys. Lett.* **2020**, *117*, 073302.
[21] J. T. Friedlein, R. R. McLeod, J. Rivnay, *Org. Electron.* **2018**, *63*, 398.
[22] A. Weltman, J. Yoo, E. Meng, *Micromachines* **2016**, *7*, 180.
[23] J. T. Friedlein, J. Rivnay, D. H. Dunlap, I. McCulloch, S. E. Shaheen, R. R. McLeod, G. G. Malliaras, *Appl. Phys. Lett.* **2017**, *111*, 023301.
[24] D. A. Bernards, D. J. Macaya, M. Nikolou, J. A. DeFranco, S. Takamatsu, G. G. Malliaras, *J. Mater. Chem.* **2008**, *18*, 116.
[25] L. Kergoat, L. Herlogsson, B. Piro, M. C. Pham, G. Horowitz, X. Crispin, M. Berggren, *Proc. Natl. Acad. Sci. USA* **2012**, *109*, 8394.
[26] S. Fabiano, S. Braun, M. Fahlman, X. Crispin, M. Berggren, *Adv. Funct. Mater.* **2014**, *24*, 695.
[27] E. W. Keefer, B. R. Botterman, M. I. Romero, A. F. Rossi, G. W. Gross, *Nat. Nanotechnol.* **2008**, *3*, 434.
[28] M. E. Obien, K. Deligkaris, T. Bullmann, D. J. Bakkum, U. Frey, *Front. Neurosci.* **2015**, *8*, 423.
[29] J. Rivnay, H. Wang, L. Fenno, K. Deisseroth, G. G. Malliaras, *Sci. Adv.* **2017**, *3*, e1601649.
[30] Y. H. Kim, A. Y. Kim, G. H. Kim, Y. H. Han, M.-A. Chung, S.-D. Jung, *Biomed. Microdevices* **2016**, *18*, 14.
[31] M. R. Abidian, J. M. Corey, D. R. Kipke, D. C. Martin, *Small* **2010**, *6*, 421.
[32] X. Luo, C. L. Weaver, D. D. Zhou, R. Greenberg, X. T. Cui, *Biomaterials* **2011**, *32*, 5551.
[33] T. D. Y. Kozai, K. Catt, Z. Du, K. Na, O. Srivannavit, R.-u. M. Haque, J. Seymour, K. D. Wise, E. Yoon, X. T. Cui, *IEEE Trans. Biomed. Eng.* **2016**, *63*, 111.
[34] H.-C. Tian, J.-Q. Liu, D.-X. Wei, X.-Y. Kang, C. Zhang, J.-C. Du, B. Yang, X. Chen, H.-Y. Zhu, Y.-N. NuLi, C.-S. Yang, *Biomaterials* **2014**, *35*, 2120.
[35] A. G. Polyravas, V. F. Curto, N. Schaefer, A. B. Calia, A. Guimera-Brunet, J. A. Garrido, G. G. Malliaras, *Flexible Printed Electron.* **2019**, *4*, 044003.